Journal Title
XX(X):2–23

DOI: 10.1177/ToBeAssigned
www.sagepub.com/
SAGE

Understanding nonlinearity in electrochemical systems using multisine-based nonlinear characterization

Chuanxin Fan[1], Thomas R. B. Grandjean[1], Kieran O'Regan[2,3], Emma Kendrick[2,3] and Widanalage D. Widanage[1,3]

Abstract

With the development of advanced characterization techniques, LIB nonlinearities have recently gained increased attention which can benefit battery health diagnosis and ageing mechanism identification. In comparison to conventional single sine-wave based methods, the multisine-based nonlinear characterization method has the advantage of capturing the dynamic voltage response within a short testing duration, and therefore has further development potential for on-board applications. However, understanding LIB electrochemical processes that contribute to battery nonlinearities is still unclear.

In this paper, the sensitivity of the Doyle-Fuller-Newman (DFN) model parameters are analysed in the frequency domain to investigate the electrochemical processes that contribute to the nonlinear dynamics of the voltage response. To begin with, the nonlinearities of the DFN model with validated parameters are characterised and compared to experimental data from a commercial cell. This demonstrated a significant difference between the mathematical model and the non-linearities determined experimentally. Then, a global sensitivity analysis (GSA) is applied to determine the most sensitive parameter contributing to battery nonlinearities. Lastly, the appropriate value of the most sensitive parameter which results in the closest nonlinear response to the commercial battery is estimated through minimizing the root mean square error (RMSE). The results show that the charge transfer coefficient is the most sensitive parameter contributing to battery nonlinearities among the DFN model parameters. The nonlinear response of the DFN model is validated with good agreement with the experimental results, when the Butler-Volmer kinetic is asymmetrical due to the unequal anodic and cathodic charge-transfer coefficients.

Keywords
Lithium-ion battery, Multisine-based nonlinear characterization, Electrochemical battery model, Nonlinear dynamic responses, Sensitivity analysis

Introduction

Electrochemical processes within a lithium-ion battery, such as charge-transfer kinetics, mass transport, and thermodynamic show dynamic nonlinear behaviour (Newman and Thomas-Alyea 2012). In lithium-ion battery (LIB) dynamics, the nonlinear behaviour manifests as a non-proportional variation relationship between the terminal voltage and the current excitation. The intensity of nonlinear behaviour, termed as nonlinearity, results in poor accuracy of conventional empirical battery models within battery management system (BMS) applications (Relan et al. 2017; Wang et al. 2020a,b). Furthermore, nonlinearities are also being utilized as a novel indicator for state-of-health (SOH) diagnosis (Harting et al. 2019). In order to achieve superior control and accurate monitoring of an advanced BMS, an in-depth understanding of battery nonlinearity, its origin, and the factors that influence it are critical.

In recent years, nonlinear characterization methods have been developed for investigations of battery nonlinearities (Murbach et al. 2018; Harting et al. 2017; Firouz et al. 2016; Fan et al. 2021). Unlike conventional techniques such as the pulse power characterisation (PPC) test and the electrochemical impedance spectroscopy (EIS) test applied in the time domain, the nonlinear characterization methods are performed in the frequency domain to capture and quantify battery nonlinearities. As a nonlinear dynamical system, the voltage response of a battery depends on the frequency content, such as harmonics, phase, amplitude, and bandwidth, of the excitation current (Widanage et al. 2016a). According to the characteristic frequency range of each electrochemical process, the processes can be distinguished and analysed separately (Wolff et al. 2019). Murbach et al. (2018) proposed a moderate-amplitude extension technique to linear EIS to provide a complementary diagnostic for the whole-battery behaviours, termed as nonlinear electrochemical impedance spectroscopy (NLEIS). Nevertheless, nonlinear frequency response analysis (NFRA), a single sine sweep based method which involves the second and the third harmonics, was first performed on lithium-ion batteries at weakly nonlinear regime to discriminate different electrochemical processes (Harting et al. 2017). Further research from Harting *et al.*

[1]WMG, University of Warwick, Coventry, CV4 7AL, United Kingdom
[2]School of Metallurgy and Materials, University of Birmingham, Edgbaston, Birmingham, BT15 2TT, United Kingdom
[3]The Faraday Institution, Quad One, Becquerel Avenue, Harwell Campus, Didcot, OX11 0RA, United Kingdom

Corresponding author:
Chuanxin Fan, WMG, University of Warwick, Coventry, CV4 7AL, UK.
Email: Chuanxin.Fan@warwick.ac.uk

applied NFRA on both fresh and aged cells to identify different degradation processes (Harting et al. 2018). Furthermore, Wolff *et al.* studied a model-based assessment of NFRA on a pseudo-two-dimensional battery model to interpret the battery nonlinear frequency response (Wolff et al. 2018). NRFA has been proven as an effective method in a laboratory environment for battery nonlinear response analysis. However, the wide frequency range of this single sine sweep based technique i.e. from mHz to MHz, results in difficulties for practical on-board applications. Within this frequency range, however, the dynamic response within the low frequency range is recognized to play a dominant role in battery behaviour (Widanage et al. 2016a).

Inspired by the frequency domain identification theory, the multisine-based nonlinear characterization methods, which focus on the low and partial medium frequency ranges, have been proposed to rapidly and accurately characterize battery dynamic responses. Firouz *et al.* applied multisine signals with various random phase realizations on to characterize the battery voltage response (Firouz et al. 2016). Focusing on nonlinearities of a cell and individual electrodes, Fan et al. (2021) performed a multisine-based characterization method using a reference electrode with diverse current root mean square (rms) values and state-of-charge (SoC) levels. Compared to NFRA, the multisine-based methods are able to drastically shorten characterization duration and offer valueable information of advanced battery modelling for BMS applications (Widanage et al. 2016b; Firouz et al. 2020). Even though nonlinearities of battery systems have been characterized by multisine-based methods, the understanding of battery nonlinear responses and the effect of complex electrochemical processes on battery nonlinearities are, however, still unclear.

Since commercial batteries are manufactured according to specific confidential recipes, it is not feasible to apply experimental tests to investigate the nonlinearity of batteries with diverse electrochemical properties. Nonetheless, mathematical battery models can achieve this goal by studying parameters of interests. The dynamic behaviour of a lithium-ion battery caused by electrochemical processes can be emulated by the governing equations (Newman and Thomas-Alyea 2012). For example, the charge-transfer kinetics on the electrode and electrolyte interface can be represented by Butler-Volmer equation, and Fick's law is widely applied to account for the diffusion process in the electrode active material (Rahn and Wang 2013). With the help of advanced experimental techniques, essential parameters can be obtained and a well parametrized lithium-ion battery (LIB) model is able to achieve high accuracy and validity (Chen et al. 2020). Subtle variations in physical parameters cause the behavior of a battery to change accordingly. Therefore, the role of each electrochemical process can be investigated by analysing the sensitivity of parameters related to battery nonlinearity.

Sensitivity analysis (SA) quantifies the uncertainty in the output of a mathematical model can be attributed to the uncertainty of model input factors' (MIF), e.g. assumptions, errors in the data, resolution, and parameters (Saltelli 2002). Liu et al. (2021a,b) proposed powerful sensitivity analysis solutions to quantify the importance of strong-coupled feature parameters, which offer reliable interpretability for the related battery applications. To date, some studies have focused on the SA of various battery models in the time domain to investigate how sensitive the model output voltage is to changes in its parameters, and SA is normally utilized for parameter

estimation and identifiability. Lai et al. (2020) investigated the sensitivities of a 2RC (resistor-capacitor) branch model with one-state hysteresis (2RCH) to determine the crucial parameters to reduce the cost of SoC estimation and retain the results accuracy. Deng et al. (2021) analysed the parameter sensitivity of a typical physics-based model for all-solid-state battery model and proposed a joint estimation method of model parameters and states. The results show that the maximum and minimum lithium-ion concentrations have the greatest influence on the model output. Grandjean et al. (2019) identified that the most sensitive parameters of a single particle model with electrolyte (SPMe) using the Morris screening method are the anode diffusion coefficient and cathode diffusion coefficient. Most of existing SA studies focus on the effect of parameters on the output of the battery model for robustness evaluation, however, very few researchers investigate the effect of physical parameters contributing to the battery nonlinearities. In (Wolff et al. 2019), the authors applied NFRA on simple fundamental models to illustrate the effect of parameters on nonlinear responses. Wolff et al. (2018) shows the nonlinear voltage responses of the Pseudo-two-Dimensional (P2D) lithium-ion battery model from several model parameters under NFRA characterization. In these two studies, only one parameter was examined while keeping the other parameters at their nominal values at a single time, which is termed as a local analysis method in the SA perspective. It is unable to detect the presence of interactions between parameters of interests (Czitrom 1999). Compared to local methods, global methods consider the sensitivity across the whole input space and study all the possible parameter combinations to evaluate the effect from parameters interactions. Therefore, global methods are universally recognized as more comprehensive methods for sensitivity analysis.

This paper has the following four contributions:

(i) A multisine-based characterization method is applied on a parametrized DFN model and a $5\ \mathrm{A\,h}$ LG M50 experimental lithium-ion cell. The dominant linear, odd and even order nonlinearity from experimental data and the DFN model are analysed and compared in the frequency domain, and a significant difference in the nonlinearities between the mathematical model and the real battery is observed.

(ii) Unlike sensitivity analysis work in the time domain, this paper applies a global sensitivity analysis on the parametrized DFN model to identify the most sensitive physical parameters to battery odd and even nonlinearities in the frequency domain, thus the related electrochemical process contributing to the nonlinearity is determined.

(iii) By minimizing the root mean square error (RMSE) by tuning the most sensitive nonlinearity related parameter obtained by the sensitivity analysis, the nonlinear and linear responses of the DFN model has a good agreement with the experiential data.

(iv) With the experimental data, this paper demonstrates how a multisine-based characterization method can assist with estimating the value of charge-transfer coefficient.

The remainder of this paper is organized as follows. In Section 2, an introduction of the multisine-based nonlinear characterization method is presented, presenting the

random phase odd multisine signal design and frequency responses analysis. Section 3 details the proposed method for investigating the nonlinear and dominant linear dynamic responses of the DFN model and the global sensitivity analysis method. Section 4 discusses the sensitivity analysis results of the parameters that contribute to the odd and even order nonlinearities and the dominant linear response, and it also presents the effect of the physical parameters on the battery frequency responses. Finally, Section 5 concludes the paper.

Multisine-based characterization method

Random phase odd multisine signal

In this work, to capture battery dynamic responses, a parametrized DFN model and three 3-electrode configuration LGM50 $5\,\mathrm{A\,h}$ experimental cells were excited and characterised with a multisine-based nonlinear characterization method from our group's previous study (Fan et al. 2021). As a periodic broadband signal (a signal that repeats), the multisine signal is designed by summing sinusoids, which provides flexibility in the design of its amplitude spectrum and harmonic content (Schoukens et al. 2012). A general multisine excitation signal can be expressed as Equation (1).

$$u(n) = \sum_{k=1}^{K} A_k \sin\left(2\pi n k f_s/N + \varphi_k\right) \qquad n = 0, ..., N-1 \tag{1}$$

Where N is the number of samples per period, K denotes the highest harmonic number of the signal, f_s is the sampling frequency, A_k is the amplitude and φ_k is the phase of the k^{th} harmonic. The N of a multisine can be flexibly determined and the frequency resolution is set to $f_0 = f_s/N$ Hz. According to the Shannon sampling theorem, the highest possible harmonic K has to be less than or equal to $N/2$. Thus, the highest possible frequency of the multisine signal can be equal to the product $f_0 \times K$ and should span the characteristic frequency range of battery nonlinear behaviour for characterization. To ensure the cell's steady state at a fixed SoC during the characterization tests, the DC frequency, which is $n = 0$ harmonic, is suppressed for obtaining a zero-mean current signal.

When a multisine signal is applied to a nonlinear system (battery included), some energy injected at the excited harmonics in the excitation signal will be transferred and observed at the other harmonic positions in the output spectrum, which indicates the system nonlinearities (Evans et al. 1994). To characterize the nonlinearity of a battery, the harmonic content f_k, harmonic phases φ_k, and amplitude spectrum A_k are the key components which require to be determined in the signal design procedure. The multisine signal is designed as an odd multisine, which randomly excites only two odd harmonics in each group of three consecutive odd harmonics and suppresses all even harmonics within the bandwidth considered. The set of excited harmonics is denoted as H_{exc} and the sets of suppressed harmonics are termed as $H_{supp,odd}$ and $H_{supp,even}$ with respect to the odd and even harmonics. The motivation of suppressing harmonics is that the suppressed odd and even harmonics can be utilized for detecting the odd and the even order nonlinearities, respectively (Widanage et al. 2012). The phases of the excited harmonics can be set to obtain different amplitude distributions

to excite the dynamics around a certain operating point (Schoukens and Dobrowiecki 1998; Pintelon and Schoukens 2012). Depending on technical constraints such as tester current and voltage limitation and safety issues (cell temperature, over and under voltage), large peaks of a designed signal should be minimized, multisine thus can be optimized by minimising a phase-related criterion known as the crest factor (CF) (Zappen et al. 2018). In addition, the amplitudes A_k are identical to unit across all the excited harmonics (a flat spectrum), and the root-mean square (rms) value of the designed multisine signal can be scaled in the time domain for a specific amplitude.

In this study, the bandwidth of the odd random phase multisine signal was set as $10\,\mathrm{Hz}$ to include the low and partial mid characteristic frequency ranges, such that the dominant nonlinearities caused by both diffusion and charge-transfer kinetics behaviour can be characterized (Fan et al. 2021). Given that the sampling frequency f_s of the hardware is $50\,\mathrm{Hz}$, the number of sample per period N is set to $N = 5000$ giving a signal periods of $100\,\mathrm{s}$. The frequency resolution is therefore $f_0 = 1/100$ Hz. A total 334 odd harmonics out of all $K = N/2 = 2500$ harmonics were excited giving $H_{exc} = \{1, 5, 7, 9, 13, 15, 21, 23, ..., 999\}$ within the bandwidth ($10\,\mathrm{mHz}$ to $10\,\mathrm{Hz}$). To improve the robustness of the characterization results, the periodic input multisine signal $u(n)$ is repeated total $P = 10$ times per SoC and thus the total duration will be $T_{total} = P \times 100\,\mathrm{s} = 1000\,\mathrm{s}$ at any given SoC. In addition, the designed random phase φ_n of the excited harmonics is a uniformly distributed random variable between 0 to 2π. Nevertheless, since the experimental cells in this work only requires quite small input current ($11.5\,\mathrm{mA}$ as 1 C-rate) for characterization, the CF optimization problem is not necessary and thus out of scope. To compare with NFRA (Harting et al. 2017), the rms of the multisine signal was set as $17.25\,\mathrm{mA}$ (1.5C) in this study.

Frequency domain dynamic responses analysis

In this work, the designed multisine current signals were applied to a parametrised DFN model and three 5Ah cylindrical experimental cells. In practice, the input current $i^{[p]}(t)$ and output voltage $v^{[p]}(t)$ data will be recorded in time domain as follow:

$$i^{[p]}(n), \quad v^{[p]}(n) \qquad p = 1, 2, ..., P \quad n = 0, ..., N-1 \tag{2}$$

Where p indicates the pth period of the input signal $i(n)$ and of the output voltage response $v(n)$, and P denotes the total number of periods at each SoC which is set as 10. By fast Fourier transform (FFT), the discrete time domain data can be transformed to the frequency domain, as input and output spectrum:

$$I^{[p]}(k), \quad V^{[p]}(k) \qquad k = 0, ..., N-1 \tag{3}$$

where $I^{[p]}(k)$, $V^{[p]}(k)$ in Equation (3) denote the spectrum of $i^{[p]}(n)$, $v^{[p]}(n)$ at the k^{th} harmonic.

In the frequency domain, the spectrum of measured voltage output data can be represented as:

$$V^{[p]}(k) = V_0^{[p]}(k) + V_S^{[p]}(k) + N_V^{[p]}(k) \qquad k \in H_{exc} \tag{4a}$$

$$V^{[p]}(k) = V_S^{[p]}(k) + N_V^{[p]}(k) \qquad k \in H_{supp,odd} \cup H_{supp,even} \tag{4b}$$

Where $V_0^{[p]}(k)$ is the dominant linear voltage response of a battery which only appears on excited harmonics as shown in Equation (4a), $V_S^{[p]}(k)$ characterizes the battery nonlinearity, and $N_V^{[p]}(k)$ indicates the noise distortion from practical environment and measurement hardware in the voltage output spectrum (Pintelon and Schoukens 2012).

Based on the voltage output spectra $V^{[p]}(k)$, the mean spectra $\bar{V}(k)$ can be estimated by averaging over P periods to reduce the effect of noise, as shown in Equation (5a). Note that the P here indicates the measured periods when the battery reaches a steady state. Further, according to Equation (5b), the corresponding variance $\hat{\sigma}^2_{\bar{V}(k)}$, which suggests the uncertainty of $\bar{V}_{(k)}$, can be calculated. Statistically, the uncertainty is related to the noise of environment and hardware equipments, and the smaller variances indicates the higher reliability of characterization results. It is worth mentioning that all calculated results are shown in decibels by directly using the MATLAB command '*dB*'.

$$\bar{V}(k) = \frac{1}{P}\sum_{p=1}^{P} V^{[p]}(k) \tag{5a}$$

$$\hat{\sigma}^2_{\bar{V},k}(k) = \sum_{p=1}^{P} \frac{\left|V^{[p]}(k) - \bar{V}(k)\right|^2}{P(P-1)} \tag{5b}$$

Theoretically, the output response of a linear system will retain the same harmonics as the input signal, and only the different amplitude and phase will vary. However, for a non-linear system, intermodulation of the input signal frequencies leads to additional harmonic components in the output spectrum. Thus, odd and even order nonlinearities $\bar{V}(k)$ can be observed and quantified according to the energy shown at detection harmonics $k \in H_{supp,odd}$ and $k \in H_{supp,even}$ in the voltage response spectrum.

Method

In this work, the frequency responses of the "Doyle-Fuller-Newman" (DFN) model with published LGM50 cylindrical cells parameters referring to (Chen et al. 2020) and corresponding three physical experimental cells are characterized by the multisine-based characterization method. The sensitivity of the physical parameters on the battery nonlinearities is analysed and ranked using global sensitivity analysis methods to identify the most sensitive parameter and electrochemical process.

Electrochemical Model

The "Doyle-Fuller-Newman" (DFN) model proposed by Doyle et al. (1993), which has been widely applied in the field of lithium-ion battery research, is utilized in this work as a physics based electrochemical battery model. Fig. 1 illustrates the modelling approach for a Li-ion cell. The DFN model implements two dimensions, particle level r and cell level x dimensions, to represent the dynamic behaviour of a lithium-ion battery. In the r dimension, Li-ions diffusion behaviour within the particles

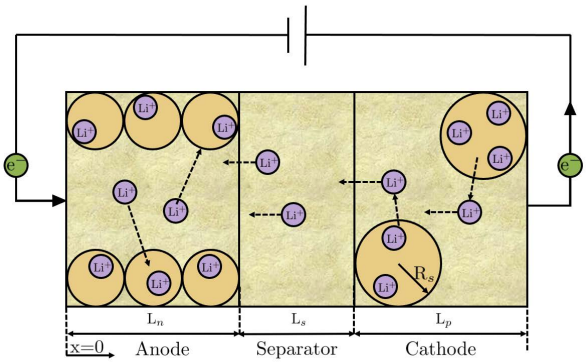

Figure 1. DFN modelling approach for a Li-ion cell. Adapted from Khalik et al. (2021).

of cathode and anode are modelled by mathematical equations. Furthermore, a lithium-ion cell is divided into three regions, namely the cathode, the separator, and the anode in the x dimension. Li-ions exist in both solid and electrolyte phases in the electrodes, but only in the liquid phase in the separator. In the solid phase, Li-ions are intercalated into the solid-phase material, which is represented by spheres with radius R_s. In the liquid phase, Li-ions exist in a dissolved state in the electrolyte. Li-ions' intercalation and deintercalation between the solid particles in the cathode and anode define the charging and discharging of a lithium-ion battery. The governing equations and boundary conditions of the DFN model are

$$\frac{\partial c_{s,k}}{\partial t} = \frac{D_{s,k}}{r^2}\frac{\partial}{\partial r}\left(r^2\frac{\partial c_{s,k}}{\partial r}\right) \tag{6a}$$

$$\left.\frac{\partial c_{s,k}}{\partial r}\right|_{r=0} = 0, \quad \left.-D_{s,k}\frac{\partial c_{s,k}}{\partial r}\right|_{r=R_s} = j_k \tag{6b}$$

$$\varepsilon_{e,k}\frac{\partial c_{e,k}}{\partial t} = \frac{\partial}{\partial x}\left(D_e\varepsilon_{e,k}^b\frac{\partial c_{e,k}}{\partial x}\right) + \frac{3\varepsilon_{s,k}\left(1-t^+\right)}{R_k}j_k \tag{7a}$$

$$\left.\frac{\partial c_{e,n}}{\partial x}\right|_{x=0} = \left.\frac{\partial c_{e,p}}{\partial x}\right|_{x=L} = 0 \tag{7b}$$

$$\frac{\partial}{\partial x}\left(\sigma_{s,k}\varepsilon_{s,k}\frac{\partial \phi_{s,k}}{\partial x}\right) = \frac{3\varepsilon_{s,k}F}{R_k}j_k \tag{8a}$$

$$\left.\sigma_{s,n}\varepsilon_{s,n}\frac{\partial \phi_{s,n}}{\partial x}\right|_{x=0} = \left.\sigma_{s,p}\varepsilon_{s,p}\frac{\partial \phi_{s,p}}{\partial x}\right|_{x=L} = \frac{i_{app}}{A_{surf}} \tag{8b}$$

$$\left.\sigma_{s,n}\varepsilon_{s,n}\frac{\partial \phi_{s,n}}{\partial x}\right|_{x=L_n} = \left.\sigma_{s,p}\varepsilon_{s,p}\frac{\partial \phi_{s,p}}{\partial x}\right|_{x=L-L_p} = 0 \tag{8c}$$

$$\frac{\partial}{\partial x}\left(\kappa\varepsilon_{e,k}^b\frac{\partial \phi_{e,k}}{\partial x} - \kappa\varepsilon_{e,k}^b\frac{2(1-t^+)RT}{F}\frac{\partial \ln c_{e,k}}{\partial x}\right) = -\frac{3\varepsilon_{s,k}F}{R_k}j_k \tag{9a}$$

$$\left.\frac{\partial \phi_{e,n}}{\partial x}\right|_{x=0} = \left.\frac{\partial \phi_{e,p}}{\partial x}\right|_{x=L} = 0 \tag{9b}$$

$$j_k = \begin{cases} \frac{i_{0,k}}{F}(\exp(\frac{\alpha_a F}{RT}\eta) - \exp(-\frac{\alpha_c F}{RT}\eta)), & k \in \{n,p\}, \\ 0, & k = s. \end{cases} \tag{10a}$$

$$i_{0,k} = k_k c_e^{\alpha_a} \left(c_{s,k}^{max} - c_{s,k}|_{r=R_k}\right)^{\alpha_a} \left(c_{s,k}|_{r=R_k}\right)^{\alpha_c} \tag{10b}$$

$$\eta = \phi_{s,k} - \phi_{e,k} - U_k(c_{s,k}|_{r=R_k}), \qquad k \in \{n,p\} \tag{10c}$$

$$U(t) = \phi_{s,p}(L,t) - \phi_{s,n}(0,t) - \frac{R_f^k}{A_{surf}} i_{app}(t) \tag{11}$$

The readers can refer to (Doyle et al. 1993) for more details of the DFN model. In this work, the electrochemistry-based battery modelling toolbox proposed by Khalik et al. (2021), which allows the user to easily toggle between constant and time-varying parameters, was applied to perform the simulation of the DFN model in MATLAB R2019b.

The parameters that contribute to the nonlinear behaviour were selected for evaluation which is explained in the following sections. The potential sources of nonlinearity in a nonlinear system can be attributed to inherent nonlinear functions or time-varying parameters in linear functions. For example, the Butler-Volmer equation Equation (10), which describes the electrochemical kinetics on electrodes, is a typical nonlinear function in the DFN model system. Given that the inherent property of nonlinear functions, small perturbations on the parameters in Equation (10) should lead to a change of the system nonlinearity. Therefore, the charge transfer coefficients α and the reaction rate coefficient k_0 were considered as model input factors (MIFs) for the sensitivity analysis in this study. In contrast to many SA literatures on electrochemical models which set α_a (anodic charge transfer coefficient), α_c (cathodic charge transfer coefficient) equal to 0.5 by default, this study evaluates system nonlinearities when α_a is randomly selected within a range around the nominal value point 0.5 and then α_c equals to $1 - \alpha_a$. Note that, for the sake of simplicity, the charge transfer coefficients are set to be the same for cathode and anode. Furthermore, the reaction rate constant k was separated to cathode reaction rate coefficient k_p and anode reaction rate coefficient k_n. To implement the DFN model, spatial discretization has to be applied on the governing PDEs of Equation (6) to Equation (9), after which the resulting set of linear differential algebraic equations (DAEs) describe the diffusion of lithium-ion concentration and potential of phases. In many modelling literatures, the parameters of the solid diffusion coefficient $D_{s,k}$, electrolyte diffusion coefficient D_e and ionic conductivity κ are assumed as constant values for calculation simplicity. However, referring to (Chen et al. 2020), the experimental results show that these parameters are time-varying as they are functions of lithium-ion concentration. Therefore, the variation of these concentration-dependent parameters also act as a source of non-linearity towards the voltage response. All the seven nonlinearity related parameters in this study are defined in Table 1, and the other parameters in the governing equations have negligible effect on battery nonlinearity, which will be verified in the following sections. In addition, the aim of this work is to investigate the effect of parameters

Table 1. Nonlinearity related parameters - model input factors (MIFs).

Parameters	Dimension	Nominal Value*	Possible range
α_a	$-$	0.5	$[0.4-1.6]*Nom.$
α_c	$-$	0.5	$1-\alpha_a$
κ	Sm^{-1}	0.9487	$[0.5-1.5]*Nom.$
$D_{s,n}$	m^2s^{-1}	3.3×10^{-14}	$[0.5-1.5]*Nom.$
$D_{s,p}$	m^2s^{-1}	4×10^{-15}	$[0.5-1.5]*Nom.$
D_e	m^2s^{-1}	1.7×10^{-10}	$[0.5-1.5]*Nom.$
k_n	$Am^{2.5}mol^{-1.5}$	6.48×10^{-7}	$[0.5-1.5]*Nom.$
k_p	$Am^{2.5}mol^{-1.5}$	3.42×10^{-6}	$[0.5-1.5]*Nom.$

*Note Nom. is the abbreviation of Nominal Value.
*All other parameters used in the DFN model are refereed to (Chen et al. 2020).

to the battery nonlinearity at specific operating points. Therefore, a sufficiently wide range was selected while the DFN model is able to emulate the behaviour of a physical lithium-ion cell.

The DFN model was validated with data from an experimental cell, named as cell3, from (Fan et al. 2021) at 50% SoC while the multisine signal was set as 1.5 C-rate, as shown in Fig.2. A good agreement between the terminal voltage of the experimental data and of simulation is observed in Fig.2a. Furthermore, a $10\,\mathrm{s}$ segment is randomly selected and locally amplified, and it shows that the DFN model has minor overestimation by maximum $0.12\,\mathrm{V}$ at peak voltage. Fig.2b shows the voltage error which is determined by the estimated value subtracted by the measured value. The black dashed lines in Fig.2b include the $50\,\mathrm{mV}$ and $-50\,\mathrm{mV}$ error boundaries, and most of the voltage error is within the boundaries. Additionally, the voltage root mean square error (RMSE) of the DFN model is calculated over the entire testing period and is equal to $0.0496\,\mathrm{V}$. By using the validated model the SA is more relevant since the nominal values about which the parameters are perturbed is realistic with the commercial cell.

Sensitivity Analysis Method

In this work, the root mean square (rms) of the odd order order nonlinearity $V_{rms,odd}$ and the even order nonlinearity $V_{rms,even}$ are calculated for sensitivity analysis, while the nonlinearities of the DFN model with nominal values have been characterized by the multisine-based method, as shown in Equation (12).

$$V_{rms,l}\left(\bar{\theta}_i\right) = \sqrt{\frac{\sum_k \left(V_k\left(\bar{\theta}_1,...,\bar{\theta}_i,...,\bar{\theta}_m\right)\right)^2}{Cardinal(k)}}, \quad k \in \begin{cases} H_{supp,odd}, & l = odd \\ H_{supp,even}, & l = even \end{cases} \tag{12}$$

Where $V_{rms,l}$ is the root mean square (rms) of the voltage harmonics (suppressed odd or even harmonics), $\bar{\theta}$ denotes the nominal value, subscript i is the i^{th} parameter,

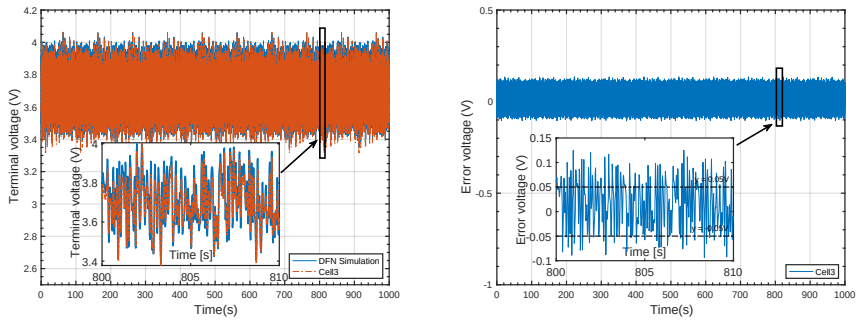

(a) **(b)**

Figure 2. DFN model prediction vs experimental data at 50% SoC under 1.5C multisine signal. (a) Terminal voltage between the DFN model and cell3; (b) Error voltage between the DFN model and cell3. The simulation result of the DFN model has a good agreement with the experimental result of three cells, which indicates the high accuracy of the parametrized DFN model in this study.

and $Cardinal(k)$ indicates the total number of odd or even detection harmonics. The root mean square (rms) is a well-known measure in engineering, also for total harmonic distortion, and it gives a sound mean value of overall nonlinearity of a system (Wolff et al. 2019; Mao et al. 2010).

The global sensitivity analysis method proposed by Morris (1991) was utilized in this work. The Morris method has been recognized as the simplest screening method to classify related parameters in a model into three sensitivity categories (Deng et al. 2021; Iooss and Lemaître 2015). Suppose each parameter $\theta_i, i = 1, 2, ..., m$ in the DFN model is independent and varies in the m-dimensional unit cube, the elementary effect (EE) of the i^{th} parameter on the output is defined as,

$$EE_i^{(r)} = \left| V_{rms,l}\left(\bar{\theta}_i^{(r)} + \Delta_i^{(r)}\right) - V_{rms,l}\left(\bar{\theta}_i^{(r)}\right) \right| \tag{13}$$

Where r realizations in the parameter space to reduce the number of model executions, and each realization is composed of $m+1$ points. In this work, 15 realizations were conducted for the sensitivity analysis of a parameter. $\bar{\theta}_i^{(r)}$ denotes the nominal value in the r^{th} realization, $\Delta_i^{(r)}$ denotes the random perturbation value from the standard uniform distribution on the open interval (0,1) and $\bar{\theta}_i^{(r)} + \Delta_i^{(r)}$ is always within the corresponding possible range as listed in Table. 1. The mean and standard deviation of elementary effect (EE) distribution is then calculated to evaluate the sensitivity of parameters. A high value of mean μ generally indicates a parameter with great influence on the output, and a high value of standard deviation σ shows the extent of nonlinear effects and/or interactions effect.

$$\mu_i = \frac{1}{r}\sum EE_i^{(r)} \tag{14a}$$

$$\sigma_i = \frac{1}{r-1} \sum \left(EE_i^{(r)} - \mu_i \right)^2 \tag{14b}$$

More details can be found in reference (Grandjean et al. 2019; Iooss and Lemaître 2015).

Results and discussion

Comparison of battery frequency responses

In this section, the results analysis and discussion mainly focus on the nonlinearity of the DFN model and experimental cells at 10% SoC. The motivation is that, as mentioned in (Fan et al. 2021), the battery nonlinearity is much stronger at low SoC points than at higher SoCs. The terminal voltage spectrum characterized by multisine-based method of DFN model with nominal parameters and the experimental cells at 1.5 C-rate 10% SoC are plotted in Fig.3. As mentioned in the signal design section, the energy shown at the excited harmonics (blue curve) indicates the dominant linear response spectrum of systems at the operating point. Corresponding to the non-excited detection harmonic positions, the level of nonlinear contributions, termed as the battery nonlinearity, can be separated to odd (red circle) and even (yellow triangle) order, respectively. The level of purple points is related to the noise standard deviation from measurement and environment error. It can be noticed that the dominant linear response spectrum (blue) and the noise floor (purple) in the DFN model agrees well with the experiment results. However, there are significant differences in the nonlinear contributions in the DFN model compared to the experimental results. The dominant nonlinearity in the DFN model is the odd nonlinearity in the whole characterization frequency range, while it is the even nonlinearity in the experiment. Given that the DFN model is commonly accepted as the most complete physical-based battery model, we assume that the model is able to fully reflect all physical characteristics of a lithium-ion battery, including the nonlinear response. Therefore, the inconsistent phenomena may be due to the inappropriate parameters in the DFN model, which motivates further investigation using sensitivity analysis in this work.

Global Sensitivity Analysis - Morris Method

Fig.4a depicts the parameter sensitivity analysis results to battery odd nonlinearity at 1.5 C-rate 10% SoC. In the SA results, the value of μ and σ can be classified into three categories, such as large, average, and minor. The MIF, which has the largest μ and σ, is deemed as the most sensitive factor and marked with a diamond. The minor level, marked with a dot, is when the value of μ and σ are less than $1/10$ of the most sensitive factor, and the MIFs can be considered insensitive. The remaining factors between 'large' and 'minor' levels are defined as average sensitivity MIFs and marked with a square. Therefore, it is observed that the charge transfer coefficient α is the most sensitive parameter and has strong non-linear effects and/or interactions effect (large μ and large σ). Note that the charge transfer coefficient α in the legend denotes the anodic charge transfer coefficient α_a. The anode reaction rate constant k_n has average non-linear effects and/or interactions effect (average $\mu = 3.49\,\mathrm{dB}$ and average $\sigma = 3.05\,\mathrm{dB}$). The remaining parameters, such as ionic conductivity κ, cathode reaction rate

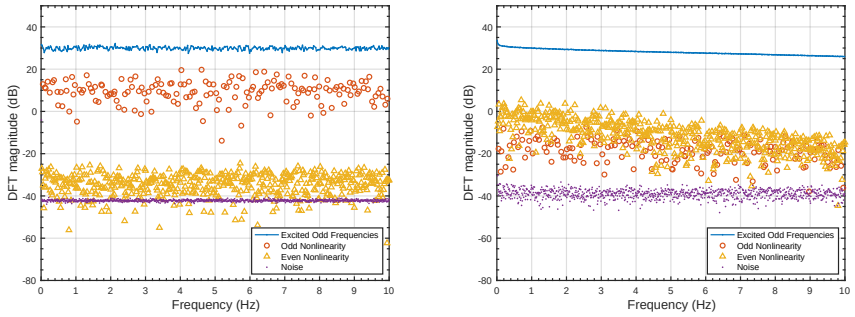

Figure 3. Comparison of terminal voltage spectrum at 1.5 C-rate 10% SoC. (a) Voltage spectrum of the DFN model; (b) Voltage spectrum of experimental data.

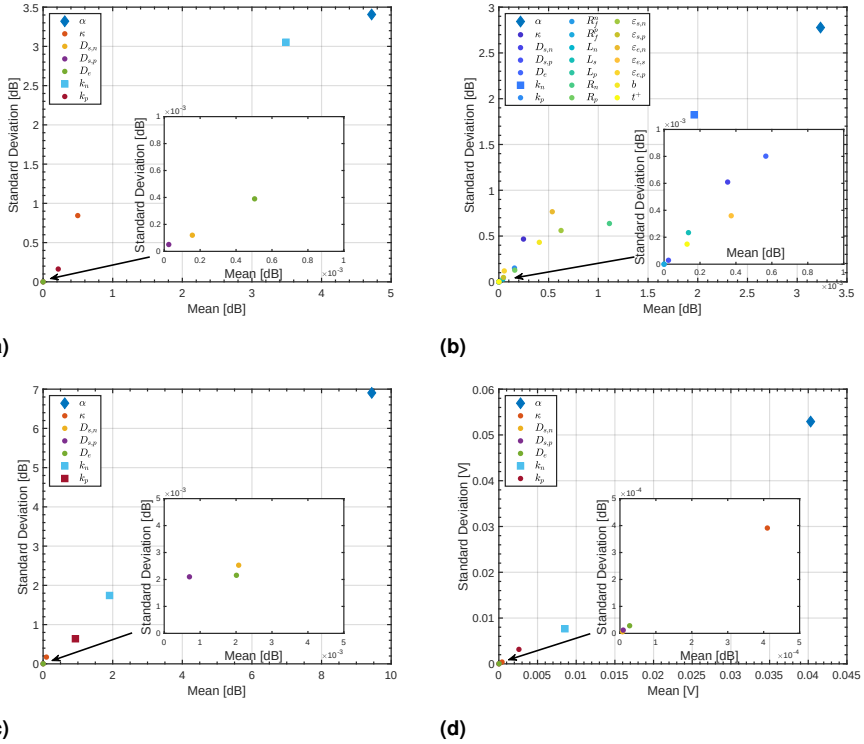

Figure 4. Parameters sensitivity analysis results of a full cell (FC) based on the Morris screening method at 1.5 C-rate 10% SoC. (a) Sensitivity of nonlinearity related parameters to odd nonlinearity; (b) Sensitivity of extended physical parameters to odd nonlinearity; (c) Sensitivity of nonlinearity related parameters to even nonlinearity; (d) Sensitivity of nonlinearity related parameters to terminal voltage.

constant k_p, cathode diffusion coefficient $D_{s,p}$, anode diffusion coefficient $D_{s,n}$, and electrolyte coefficient D_e, are insensitive towards the odd distortions observed in the spectrum, since the value of μ and σ of these MIFs are one order of magnitude smaller than the most sensitive parameter (μ<0.47 dB). The sensitive parameters α_a and k fulfil their roles in the Butler-Volmer equation, which indicates that any slight variation of the charge transfer behaviour can lead to considerable change of battery nonlinear response. Since the Butler-Volmer kinetic is an odd symmetric function (between the over-potential and current density) and shows point symmetry in the nonlinear current voltage relation with $\alpha_a = \alpha_c = 0.5$, it's reasonable to observe the variation of battery nonlinearities when the α_a is no longer 0.5 and the Butler-Volmer kinetics is not symmetric anymore.

To further validate the nonlinearity related parameters, the sensitivity of an extended physical parameters space is analysed at the same condition, as shown in Fig.4b. This extended parameters space consists of the 7 aforementioned nonlinearity related parameters and 14 extra physical parameters (See Table 3 in Supplemental material section) which are normally taken into account in electrochemical model SA studies. Consistent with Fig.4a, the most sensitive parameter in the extended parameters case is still the charge transfer coefficient α followed by the anode reaction rate constants k_n, which means the selection of nonlinearity related parameters is reasonable and the major source of battery nonlinearities is charge transfer reaction. Furthermore, Fig.4b verifies that the extended physical parameters have neglectable effect to battery nonlinearities. From a computational perspective, applying the global sensitivity analysis method on the DFN model is relatively costly, for instance, a total of 5188 s operation time was required for the 7 parameters case using a standard laptop. Given that the most sensitive parameter is included in both cases, the 7 parameters case for subsequent analysis is utilized in this work, rather than the extended 21 parameters, to reduce computational cost by two-thirds.

The sensitivity analysis results of nonlinearity related parameters to battery even nonlinearity are shown in Fig.4c. It is observed that the sensitivity of the charge transfer coefficient α is again the greatest, followed by those of anode reaction rate constant k_n and cathode reaction rate constant k_p, and the other parameters are insensitive.

The sensitivity of the parameters towards the terminal voltage are analysed by the same method used on the nonlinearity and shown in Fig.4d. The results show that the charge transfer coefficient α is the most sensitive parameter to terminal voltage, followed by anode reaction rate constants k_n and cathode reaction rate constants k_p. The charge transfer coefficient α has strong interaction effects (large μ and large σ). The anode reaction rate constant k_n and cathode reaction rate constant k_p have average non-linear effects and/or interactions effect (average $\mu = 5.57$ mV and average $\sigma = 5.41$ mV). The remaining parameters, such as cathode diffusion coefficient $D_{s,p}$, anode diffusion coefficient $D_{s,n}$, electrolyte coefficient D_e, and ionic conductivity κ, are deemed to have no effect since they are one order of magnitude smaller than α (μ<0.41 mV). Furthermore, compared to the literature which analyze the sensitivity to model voltage output in the entire SoC window (Grandjean et al. 2019), the sensitivity of the solid diffusion coefficients D_s is insensitive. The reason may be due to the variation of SoC is negligible during a multisine-based characterization test, which leads to the effect of diffusion behaviour to terminal voltage being minor.

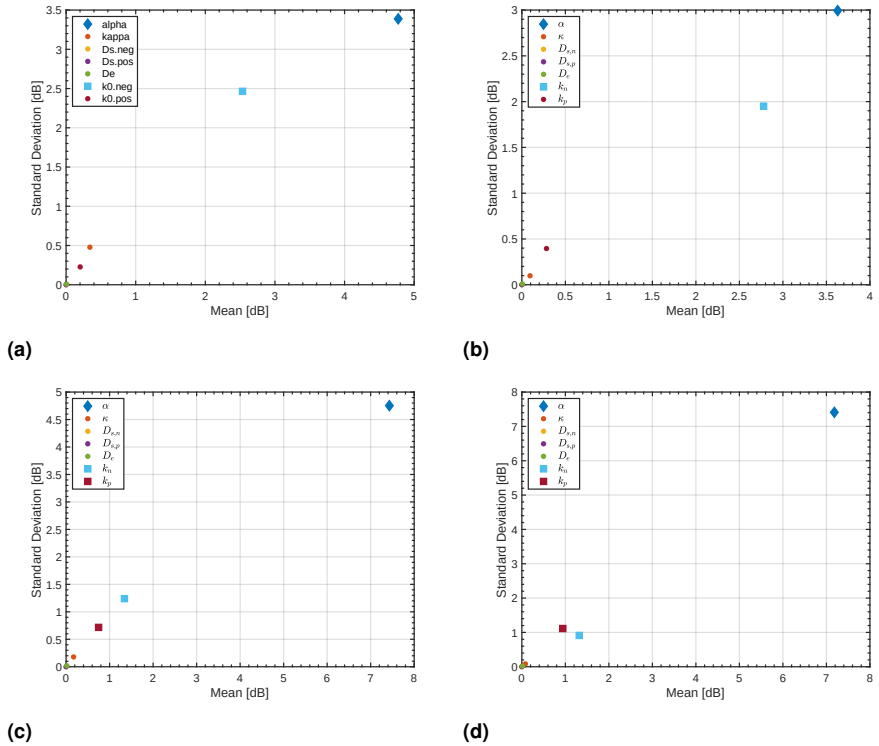

Figure 5. Sensitivity results of nonlinearity related parameters to nonlinearities at various SoC levels of; (a) Odd nonlinearity at 50% SoC, (b) Odd nonlinearity at 90% SoC, (c) Even nonlinearity at 50% SoC, and (d) Even nonlinearity at 90% SoC .

Furthermore, Fig.5 presents the sensitivity results of nonlinearity related parameters to the odd and the even order nonlinearity at 50% SoC and 90% SoC. In the Morris method, as the perturbation part Δ_i of a MIF in Equation (12) is randomly selected from the corresponding possible range, the sensitivity results of a MIF slightly varies within a certain extent. However, overall, the sensitivity of each nonlinearity related parameter are still consistent with the 10% SoC case. In addition, the cathode reaction rate constant k_p have average non-linear effects and/or interactions effect only in all even nonlinearity SA results, the reason leads to these results requires further research.

The results shown in Fig.4 and Fig.5 reveal that the charge transfer coefficient α is the most sensitive parameter to nonlinearities of a lithium-ion battery. Moreover, the sensitivity analysis results indicate that the charge-transfer reaction plays a vital role in the lithium-ion battery dynamic response at a specific level.

Effect of charge transfer coefficient α to battery nonlinearities

Based on the sensitivity analysis results, the charge transfer coefficient α has been identified as the most sensitive parameter towards the battery nonlinearity and terminal

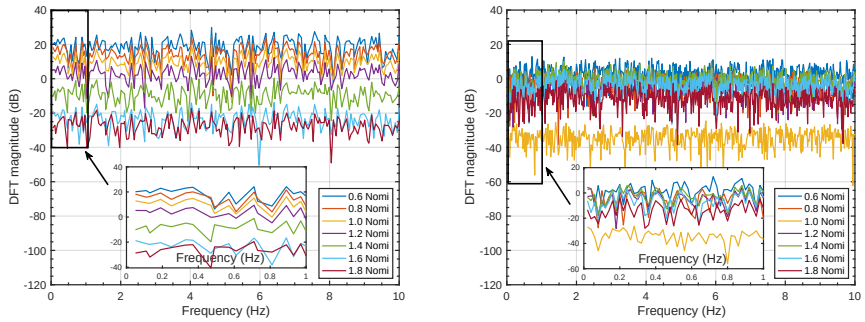

Figure 6. Nonlinearities comparison at various α_a values at 1.5 C-rate 10% SoC. (a) Odd nonlinearity comparison with various α_a; (b) Even nonlinearity comparison with various α_a.

voltage response at a specific SoC level. To further understand the effect of charge transfer coefficient α, the nonlinearities of the DFN model with various charge transfer coefficients α are characterized and compared in this section, as shown in Fig.6. The nominal values of the anodic charge transfer coefficient α_a and cathodic charge transfer coefficients α_c are 0.5, and the level of nonlinearity at nominal values are the yellow lines in the Fig.6a and Fig.6b. The anodic charge transfer coefficient α_a is varied by multiplying the nominal value by a gain factor, where the range of gain factors is defined from 0.6 to 1.8. It leads to the anodic charge transfer coefficients α_a examined in this section between 0.3 and 0.9. Then, the corresponding cathodic charge transfer coefficients α_c can be obtained by $1-\alpha_a$. While for a simple one electron transfer reaction, the sum of α_a and α_c equals to 1 is rational (Bockris and Nagy 1973).

The battery odd nonlinearities with various α_a with a odd random phase multisine current rms (as described in Section 2) at 1.5 C-rate 10% SoC were compared in Fig.6a. It clearly shows that the odd nonlinearity shifts in the interval from around $-30\,\mathrm{dB}$ to $20\,\mathrm{dB}$ in accordance with the variation of α_a. As α_a increases from the nominal value of 0.5 (1.0 Nomi (yellow line) in Fig.6a), the magnitude of the odd nonlinearity simultaneously decreases. Moreover, the odd nonlinearity increases when α_a decreases from the nominal value. Unlike the effect to odd nonlinearities, the even nonlinearities excited by the same charge transfer parameters do not increase or decrease continuously with the decrease or increase in nominal value, as shown in Fig.6b. The DFN model with the nominal value excites the weakest even nonlinearity which is at around $-35\,\mathrm{dB}$. Furthermore, the even nonlinearities of all the other cases are stronger than the nominal value case and vary between $-10\,\mathrm{dB}$ to $20\,\mathrm{dB}$. This interesting phenomena of the even nonlinearity was also noticed by Wolff et al. (2019) when the NFRA was applied on the Butler-Volmer equation. When α_a is not 0.5, the perfectly symmetric charge-transfer reaction will not exist, thereby leading to an increase of the even nonlinearity. To get a further understanding of charge transfer symmetry in the linear and nonlinear voltage response, a Taylor series expansion can be carried out to the Butler-Volmer equation Equation (10a),

$$j = \frac{i_{0,k}}{F}(\exp(\frac{\alpha_a F}{RT}\eta) - \exp(-\frac{\alpha_c F}{RT}\eta)), \quad k \in \{n, p\}, \tag{15}$$

and the first three dominant terms are contained for a comprehensive analysis of even and odd order higher harmonics,

$$\begin{aligned} j = &\left[\frac{i_{0,k}}{F}\left(\frac{(\alpha_a + \alpha_c)F}{RT}\right)\right]\eta + \left[\frac{i_{0,k}}{F}\left(\frac{(\alpha_a^2 - \alpha_c^2)F^2}{2!R^2T^2}\right)\right]\eta^2 \\ &+ \left[\frac{i_{0,k}}{F}\left(\frac{(\alpha_a^3 + \alpha_c^3)F^3}{3!R^3T^3}\right)\right]\eta^3 + \mathcal{O}(\eta^4) \end{aligned} \tag{16}$$

where $i_{0,k}$ is the exchange current density, η is the overpotential, α_a and α_c are the anodic and cathodic transfer coefficients, and F, R, and T are Faraday's constant, the gas constant, and the temperature, respectively. In this Taylor series expansion, the first three terms in right-hand side of Equation (16) can be classified into the linear term, the even nonlinear term, and the odd nonlinear term which are related to linear response as well as even and odd nonlinearities with respect to the order of independent variable η (Pintelon and Schoukens 2012), and the reminder term $\mathcal{O}(\eta^4)$ is neglected. Given that the assumption $\alpha_a + \alpha_c = 1$, the change of α_a and α_c will not affect the first linear term. However, the variation of charge transfer coefficients will influence the second and third terms in Equation (16), especially the second term which is related to the even nonlinearity. For many electrochemical model studies using the values $\alpha_a = \alpha_c = 0.5$ indicate a symmetric charge-transfer kinetic, the even nonlinear term in Equation (16) is totally eliminated which can interpret the reason that the extremely minor magnitude of even nonlinearity in the DFN model simulation in Fig.3a. In the case of $\alpha_a \neq \alpha_c$ caused by the asymmetric charge-transfer reaction, the even nonlinear term appears and leads to the even nonlinearity in the results of the nonlinear characterization. As the difference between α_a and α_c increases, the factor $(\alpha_a^2 - \alpha_c^2)$ of the even nonlinear term will increase which will excite the greater even nonlinearity as shown in Fig.6b. Compared to the even nonlinear term, the odd nonlinear term (in Equation (16)) will always be present due to the summation of $\alpha_a^3$and α_c^3. However, the physical interpretation of the even and odd nonlinearities is still an open question which requires further research.

Refer to the content shown in Fig.6, the nonlinear response of the DFN model could approach to the experimental results by tuning the charge transfer coefficients to an appropriate value. For example, Fig.7 shows the terminal voltage spectrum from the DFN model with $\alpha_a = 0.8$ and $\alpha_a = 0.9$ at 10% SoC. In Fig.7a, the odd and even nonlinearities are overlapped over the whole characterization frequency, which is consistent with the experimental data especially at high frequency range 6 Hz to 10 Hz. On the contrary, it can be noticed that the level of odd and even nonlinear contributions in the low frequency range from 10 mHz to 4 Hz are roughly comparable to the experimental case shown in Fig.3b. Further, the even nonlinear is now the dominant nonlinearity in the DFN model which is the opposite of the case with $\alpha_a = 0.5$ (See Fig.3b). However, there are still differences in shape of the nonlinearities and the linear response level of the DFN model in both Fig.7a and Fig.7b compared to the experiment results, such as the overlapping of the odd and even distortions in the high frequency

range and the 'ramp' shape curves that gradually decreases over the whole frequency range which is observed in the experimental data but not in the simulations.

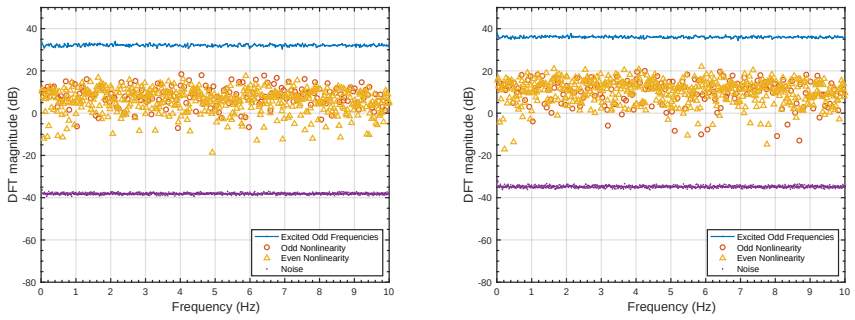

Figure 7. Terminal voltage spectrum from DFN model at 1.5 C-rate 10% SoC when (a) α_a is set at 0.8; (b) α_a is set at 0.9.

To determine the α_a value that will lead to a comparable the experimental result, the RMSE of odd and even nonlinearity of the DFN model with various α_a values are calculated and listed in Table. 2. The nonlinearity error between the model and experimental result show that, while the nominal $\alpha_a = 0.5$ is set, the DFN model's odd nonlinearity RMSE is 29.15 and at medium error level, as well as the even nonlinearity RMSE (22.20) is the largest among all various α_a value cases. This information is consistent with the results shown in Fig. 6. According to the Table. 2, the $\alpha_a = 0.8$ case results in the minimum odd nonlinearity RMSE and $\alpha_a = 0.9$ case leads to the least even nonlinearity RMSE. Compared with the nominal case, both 0.8 and 0.9 could reduce the RMSE by more than a half, which indicates that these two cases lead to a non-linear voltage response that is closer to the experimental data.

Table 2. The odd and even nonlinearity RMSE with various α_a values, while the DFN model is at 10% SoC and under 1.5 C-rate multisine signal.

α_a	**Odd Nonlinearity RMSE**	**Even Nonlinearity RMSE**
0.3	38.37	15.27
0.4	34.03	8.79
0.5*	29.15	22.20
0.6	22.53	8.33
0.7	10.48	11.33
0.8	3.98	7.87
0.9	7.80	0.41

*The nominal value of α_a refereed to (Chen et al. 2020).

Effect of charge transfer coefficient α towards the linear response

Given that the difference in the shape of voltage output spectrum, the effect of α towards linear response was further investigated in this section. Compared to Fig.3a, it can be found that the linear response (blue curve) in the Fig.7 is smoother and the 'ramp' shape of the linear response in the low frequency range is more significant than with $\alpha_a = 0.5$. Nevertheless, these two characteristics are clearly reflected in the experimental results as shown in Fig.3b, which indicates that the charge transfer coefficient α may also affect the dominant linear response.

Fig.8 shows that the dominant linear responses at various α_a when the DFN model is at 10% SoC. Firstly, the linear responses of the full cell over the whole characterization frequency range are plotted in Fig.8a. An interesting phenomena is, when the value of α_a is selected from 0.3 to 0.6, the linear response curves exhibit fluctuations from the input multisine current. On the contrary, the cases with larger α_a values, such as 0.7, 0.8, and 0.9, show relatively flat linear response curves, which is more close to the experimental results in Fig.3b. Considering that the change of α_a can lead the charge-transfer reaction to asymmetrical, the reason of this phenomena might be related to the asymmetrical reaction plays a role of a bandpass filter which affects the overpotential on solid electrolyte interfaces. In addition, compared with the linear response in Fig.3b decreasing from $30\,\mathrm{dB}$ to $25\,\mathrm{dB}$, the magnitude of linear response in Fig.8a remains almost unchanged over the bandwidth. However, as shown in Fig.8b, the decreasing 'ramp' shape curves exist when the α is large enough like 0.8 and 0.9, but only in the extremely low frequency range (less than $0.2\,\mathrm{Hz}$). The reason attributes to this difference still requires further research. From the perspective of dominant linear response, it is still reasonable to estimate α_a equals to a value from 0.8 to 0.9 rather than 0.5 for a less difference from the experimental data at 10% SOC case.

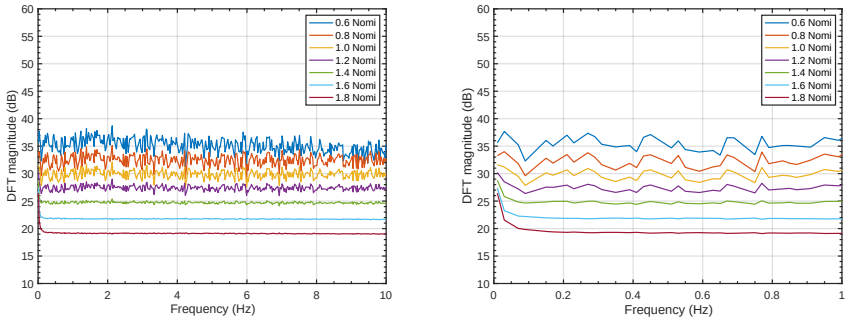

Figure 8. Dominant linear responses at various α_a values at 1.5 C-rate 10% SoC. (a) 'Fluctuating' and 'smooth' dominant linear responses in the whole characterization range; (b) 'Ramp-shaped' dominant linear responses at low frequency range.

Conclusion

This paper has applied the Morris global sensitivity analysis method on the DFN model nonlinearity, captured by a multisine-based nonlinear characterization method, to understand the electrochemical processes that contribute to battery nonlinearity. Firstly, by applying the multisine-based method, the dominant linear, odd and even nonlinearities of the parametrized DFN model were compared with experimental data. The significant difference of the nonlinear distortions suggested that the nominal value of nonlinear-related parameters may be inappropriate. Then, by applying the Morris global sensitivity analysis method, the most sensitive parameter was determined as the charge transfer coefficient α, and thus the charge-transfer kinetics is determined as the main contributor to the nonlinearity of a lithium-ion battery. Furthermore, the effects of α on the frequency domain nonlinear response were investigated by comparing the dynamic responses of the DFN model with various values of α. The results from nonlinearity RMSE show that, rather than the commonly used value of 0.5, the dynamic responses of the DFN model with α_a set as 0.8 or 0.9 provides good model agreement with the experimental data while the commercial cell is at 10% SOC. This phenomena indicates that the charge-transfer kinetics in a lithium-ion battery might be an asymmetrical behaviour, rather than the commonly assumed perfect symmetrical reaction. Lastly, this paper demonstrates the potential ability of the multisine-based characterization method to estimate the charge transfer coefficients α in the frequency domain rather than recording current voltage curves. Overall, this work enhances the understanding of lithium-ion battery nonlinear dynamic responses captured by the multisine-based characterization method and contributes to the knowledge of battery nonlinearity analysis.

In future work, the multisine-based nonlinear characterization method is to be performed on lithium-ion batteries in different health status to analysis variation of the nonlinear responses. Due to the advantages of short testing duration, it is worthy to investigate the capability of the method as an on-broad characterization technique for battery state-of-health estimation. Furthermore, though $\alpha_a = 0.8$ and $\alpha_a = 0.9$ give less frequency response error to the experimental results while the cell is at 10% SOC, the nonlinearity magnitude reduction over the frequency range observed in the experimental data is still an open question, which will be investigated in the future work.

Acknowledgements

The research presented within this paper is supported by WMG, University of Warwick, United Kingdom (09ESWM21) and Institute of Digital Engineering (IDE), United Kingdom under a grant for Virtually Connected Hybrid Vehicle project.

Declaration of conflicting interests

The authors declare that they have no known competing financial interests or personal relationships that could have appeared to influence the work reported in this paper.

Supplemental material

Table 3. Extended model input factors (MIFs) - 14 extra physical parameters for the full sensitivity analysis.

Parameters	Dimension	Nominal Value*	Possible range
R_f^n	$\Omega \times m^2$	10^{-4}	$[0.5 - 1.5] * Nom.$
R_f^p	$\Omega \times m^2$	10^{-4}	$[0.5 - 1.5] * Nom.$
L_n	m	0.9487	$[0.5 - 1.5] * Nom.$
L_s	m	3.3×10^{-14}	$[0.5 - 1.5] * Nom.$
L_p	m	4×10^{-15}	$[0.5 - 1.5] * Nom.$
R_n	m	1.7×10^{-10}	$[0.5 - 1.5] * Nom.$
R_p	m	6.48×10^{-7}	$[0.5 - 1.5] * Nom.$
$\varepsilon_{s,n}$	%	0.75	$[0.5 - 1.5] * Nom.$
$\varepsilon_{s,p}$	%	0.665	$[0.5 - 1.5] * Nom.$
$\varepsilon_{e,n}$	%	0.25	$[0.5 - 1.5] * Nom.$
$\varepsilon_{e,s}$	%	0.47	$[0.5 - 1.5] * Nom.$
$\varepsilon_{e,p}$	%	0.335	$[0.5 - 1.5] * Nom.$
b	–	1.5	$[0.5 - 1.5] * Nom.$
t^+	–	0.2594	$[0.5 - 1.5] * Nom.$

*Note Nom. is the abbreviation of Nominal Value.
*The nominal value of parameters are refereed to (Chen et al. 2020).

References

Bockris JO and Nagy Z (1973) Symmetry factor and transfer coefficient: A source of confusion in electrode kinetics. *Journal of Chemical Education* 50(12): 839–843.

Chen CH, Brosa Planella F, O'Regan K, Gastol D, Widanage WD and Kendrick E (2020) Development of Experimental Techniques for Parameterization of Multi-scale Lithium-ion Battery Models. *Journal of The Electrochemical Society* 167(8): 080534.

Czitrom V (1999) One-factor-at-a-time versus designed experiments. *American Statistician* 53(2): 126–131.

Deng Z, Hu X, Lin X, Kim Y and Li J (2021) Sensitivity Analysis and Joint Estimation of Parameters and States for All-Solid-State Batteries. *IEEE Transactions on Transportation Electrification* : 1.

Doyle M, Fuller TF and Newman J (1993) Modeling of Galvanostatic Charge and Discharge of the Lithium/Polymer/Insertion Cell. *Journal of The Electrochemical Society* 140(6): 1526–1533.

Evans E, Rees D and Jones L (1994) Nonlinear disturbance errors in system identification using multisine test signals. *IEEE Transactions on Instrumentation and Measurement* 43(2): 238–244.

Fan C, O'Regan K, Li L, Kendrick E and Widanage WD (2021) Frequency domain non-linear characterization and analysis of lithium-ion battery electrodes. *Journal of Energy Storage* 36: 102371.

Firouz Y, Goutam S, Soult MC, Mohammadi A, Van Mierlo J and Van den Bossche P (2020) Block-oriented system identification for nonlinear modeling of all-solid-state Li-ion battery technology. *Journal of Energy Storage* 28.

Firouz Y, Relan R, Timmermans JM, Omar N, Van den Bossche P and Van Mierlo J (2016) Advanced lithium ion battery modeling and nonlinear analysis based on robust method in frequency domain: Nonlinear characterization and non-parametric modeling. *Energy* 106: 602–617.

Grandjean TR, Li L, Odio MX and Widanage WD (2019) Global sensitivity analysis of the single particle lithium-ion battery model with electrolyte. *2019 IEEE Vehicle Power and Propulsion Conference, VPPC 2019 - Proceedings* .

Harting N, Wolff N and Krewer U (2018) Identification of Lithium Plating in Lithium-Ion Batteries using Nonlinear Frequency Response Analysis (NFRA). *Electrochimica Acta* 281: 378–385.

Harting N, Wolff N, Röder F and Krewer U (2017) Nonlinear Frequency Response Analysis (NFRA) of Lithium-Ion Batteries. *Electrochimica Acta* 248: 133–139.

Harting N, Wolff N, Röder F and Krewer U (2019) State-of-Health Diagnosis of Lithium-Ion Batteries Using Nonlinear Frequency Response Analysis. *Journal of The Electrochemical Society* 166(2): A277–A285.

Iooss B and Lemaître P (2015) A review on global sensitivity analysis methods. *Operations Research/ Computer Science Interfaces Series* 59: 101–122.

Khalik Z, Donkers MC and Bergveld HJ (2021) Model simplifications and their impact on computational complexity for an electrochemistry-based battery modeling toolbox. *Journal of Power Sources* 488: 229427.

Lai X, Wang S, Ma S, Xie J and Zheng Y (2020) Parameter sensitivity analysis and simplification of equivalent circuit model for the state of charge of lithium-ion batteries. *Electrochimica Acta* 330: 135239.

Liu K, Hu X, Zhou H, Tong L, Widanalage D and Marco J (2021a) Feature analyses and modelling of lithium-ion batteries manufacturing based on random forest classification. *IEEE/ASME Transactions on Mechatronics* .

Liu K, Wei Z, Yang Z and Li K (2021b) Mass load prediction for lithium-ion battery electrode clean production: a machine learning approach. *Journal of Cleaner Production* 289: 125159.

Mao Q, Krewer U and Hanke-Rauschenbach R (2010) Total harmonic distortion analysis for direct methanol fuel cell anode. *Electrochemistry communications* 12(11): 1517–1519.

Morris MD (1991) Factorial sampling plans for preliminary computational experiments. *Technometrics* 33(2): 161–174.

Murbach MD, Hu VW and Schwartz DT (2018) Nonlinear electrochemical impedance spectroscopy of lithium-ion batteries: experimental approach, analysis, and initial findings. *Journal of the Electrochemical Society* 165(11): A2758.

Newman J and Thomas-Alyea KE (2012) *Electrochemical systems*. John Wiley & Sons.

Pintelon R and Schoukens J (2012) *System Identification: A Frequency Domain Approach, Second Edition*. John Wiley and Sons. ISBN 9780470640371.

Rahn CD and Wang CY (2013) *Battery Systems Engineering*. John Wiley and Sons. ISBN 9781119979500.

Relan R, Firouz Y, Timmermans JM and Schoukens J (2017) Data-Driven Nonlinear Identification of Li-Ion Battery Based on a Frequency Domain Nonparametric Analysis. *IEEE Transactions on Control Systems Technology* 25(5): 1825–1832.

Saltelli A (2002) Sensitivity Analysis for Importance Assessment. *Risk Analysis* 22(3): 579–590.

Schoukens J and Dobrowiecki T (1998) Design of broadband excitation signals with a user imposed power spectrum and amplitude distribution. In: *IMTC/98 Conference Proceedings. IEEE Instrumentation and Measurement Technology Conference. Where Instrumentation is Going (Cat. No. 98CH36222)*, volume 2. IEEE, pp. 1002–1005.

Schoukens J, Pintelon R and Rolain Y (2012) *Mastering system identification in 100 exercises*. John Wiley & Sons.

Wang Y, Li M and Chen Z (2020a) Experimental study of fractional-order models for lithium-ion battery and ultra-capacitor: Modeling, system identification, and validation. *Applied Energy* 278: 115736.

Wang Y, Tian J, Sun Z, Wang L, Xu R, Li M and Chen Z (2020b) A comprehensive review of battery modeling and state estimation approaches for advanced battery management systems. *Renewable and Sustainable Energy Reviews* 131: 110015.

Widanage WD, Barai A, Chouchelamane GH, Uddin K, McGordon A, Marco J and Jennings P (2016a) Design and use of multisine signals for Li-ion battery equivalent circuit modelling. Part 1: Signal design. *Journal of Power Sources* 324: 70–78.

Widanage WD, Barai A, Chouchelamane GH, Uddin K, McGordon A, Marco J and Jennings P (2016b) Design and use of multisine signals for Li-ion battery equivalent circuit modelling. Part 2: Model estimation. *Journal of Power Sources* 324: 61–69.

Widanage WD, Stoev J and Schoukens J (2012) Design and application of signals for nonlinear system identification. *IFAC Proceedings Volumes* 45(16): 1605–1610.

Wolff N, Harting N, Heinrich M, Röder F and Krewer U (2018) Nonlinear Frequency Response Analysis on Lithium-Ion Batteries: A Model-Based Assessment. *Electrochimica Acta* 260: 614–622.

Wolff N, Harting N, Röder F, Heinrich M and Krewer U (2019) Understanding nonlinearity in electrochemical systems. *European Physical Journal: Special Topics* 227(18): 2617–2640.

Zappen H, Ringbeck F and Sauer DU (2018) Application of time-resolved multi-sine impedance spectroscopy for lithium-ion battery characterization. *Batteries* 4(4): 64.